IEEE Access
Multidisciplinary ⋮ Rapid Review ⋮ Open Access Journal

Received 19 April 2023, accepted 10 May 2023, date of publication 18 May 2023, date of current version 26 May 2023.

Digital Object Identifier 10.1109/ACCESS.2023.3277502

RESEARCH ARTICLE

Research on End Structure Losses and Its Suppression Method of High-Speed Canned Induction Motor

LIANLIAN GAO, SIMIN WANG, AND JIAJIA LI
School of Electrical and Electronic Engineering, Harbin University of Science and Technology, Harbin 150080, China
Corresponding author: Simin Wang (2512108552@qq.com)

This work was supported in part by the Innovative Talent Project in Heilongjiang Province under Grant UNPYSCT-2020181.

ABSTRACT In the medical and chemical fields, in order to avoid the corrosion of cores and windings, it is necessary to introduce two thin cylindrical corrosion-resistant cans and end support structures into high-speed motors. The result is that there are many kinds of losses and the internal electromagnetic distribution is complex. The loss formation mechanisms and each sort of current path are challenging to master. In order to solve this problem, a 1.5MW high-speed canned induction motor is calculated using the 3D finite element method. The superposition method is used to separate the circulating current losses and eddy current losses at the end of the motor. The mechanism and circulating current path of the circulating current losses between the structural components are analyzed. The influence of material properties of end structures on circulating current losses and path is discussed. A new circulating current losses suppression method is proposed, and the beneficial effect of the optimized structure is verified using the temperature field. This study provides a solution for the safe and reliable operation of high-speed canned induction motors.

INDEX TERMS High-speed canned induction motor, end magnetic field, circulating current losses, influencing factors.

I. INTRODUCTION

Canned motors are mainly used in nuclear, chemical, medical, and mining industries that transport toxic, corrosive, medical, or high-pressure liquids [1]. To avoid corrosion of cores and windings, a stator can and rotor can are added on both sides of the air gap [2], [3]. The can is made of corrosion resistant alloy steel, and there is a closely connected supporting structures at the ends. Under the action of the air gap and end magnetic field, the eddy current losses and circulating current losses between the can and end support structures of the high-speed canned induction motor are formed [4]. The superposition of the two types of losses not only reduces the motor's efficiency, but also tends to cause local overheating at the region of the motor. Therefore, the reliability of the motor is reduced.Therefore, it is very important to study the calculation method of eddy current losses, and their influencing factors for the preliminary structural design of high-speed canned induction motor and the safe and stable operation of the whole system.

At present, the methods of eddy current losses mainly include analytical method and finite element method. The eddy current losses of switched reluctance motor is calculated by analytical method [5]. Based on the analytical method, a new analytical method for permanent magnet eddy current loss of non-concentric pole permanent magnet synchronous motor is proposed, which considers the influence of eddy current reaction and stator slotting [6].The proposed model takes account of the influence of the output voltage harmonics from the inverter on the iron loss of the motor based on the piecewise variable coefficients method [7]. Three-dimensional boundary conditions and current vector are introduced into the subdomain model to represent the three-dimensional eddy current circulating in the magnet [8].In the analytical method, when the actual end ring resistance of the stator can is introduced, the induced current will follow a certain

The associate editor coordinating the review of this manuscript and approving it for publication was Zhengqing Yun.

elliptical path from pole to pole, rather than flowing axially along the stator core. When the end-ring resistance is considered, the loss of the stator can needs to be multiplied by k_s on the basis of the loss of the stator can without considering the end-ring resistance. k_s is the reduction factor and depends on the ratio of core length to pole pitch. In the calculation process, k_s is usually an empirical coefficient, which will cause a large error in the calculation results. The eddy current loss of permanent magnet synchronous motor is calculated by two-dimensional finite element method and three-dimensional finite element method respectively [9]. The results show that the three-dimensional finite element method is more accurate. The three-dimensional finite element method is used to analyze the influence of the leakage flux on the conductive components at the end of the motor and calculate the eddy current loss [10]. A method based on the combination of analytical method and finite element method to calculate the eddy current losses of wire windings is proposed [11]. The finite element method is used to optimize the rotor structure of the motor to reduce the rotor eddy current losses of the high-speed permanent magnet synchronous motor [12]. The three-dimensional finite element method is used to simulate the magnet segmentation, thereby reducing the eddy current losses of the permanent magnet synchronous motor [13]. A new method is proposed to reduce the rotor permanent magnet eddy current loss, the auxiliary slots with optimized size and position are proposed, which is verified by the finite element method [14].The eddy current losses and electromagnetic force characteristics of the can under the combination of two-dimensional and three-dimensional finite elements are introduced [15]. The effects of can material changes on motor losses, magnetization currents, and performance are discussed in [16], a reliable basis for the selection of can materials and performance optimization of megawatt high-speed canned induction motors is provided. The eddy current losses calculation of other structural parts at the motor end is also the focus of the research. The iron losses caused by the differences of air gap flux distribution in the coaxial cylindrical rotor layer structure is analyzed in [17]. The three-dimensional finite element method is utilized to calculate the eddy current losses in the end structural components but the paths and influencing factors of the losses is not analyzed [18], [19].The two-dimensional finite element method cannot consider the complex situation of the end structure. The current research mainly includes the calculation method of eddy current loss and the reduction of eddy current loss by changing the structure of the motor, and the eddy current path is rarely studied. Therefore, this paper uses the three-dimensional finite element method to calculate the end loss of 1.5MW high-speed canned induction motor. This method can not only calculate the eddy current loss of the motor end structure, but also calculate the circulating current losses between the metal structure parts with the superposition method. On the basis of finite element simulation, the eddy current path and circulating current path are analyzed, and a new method to reduce the end loss of the motor by blocking the circulating current path is proposed, which is verified by temperature rise.

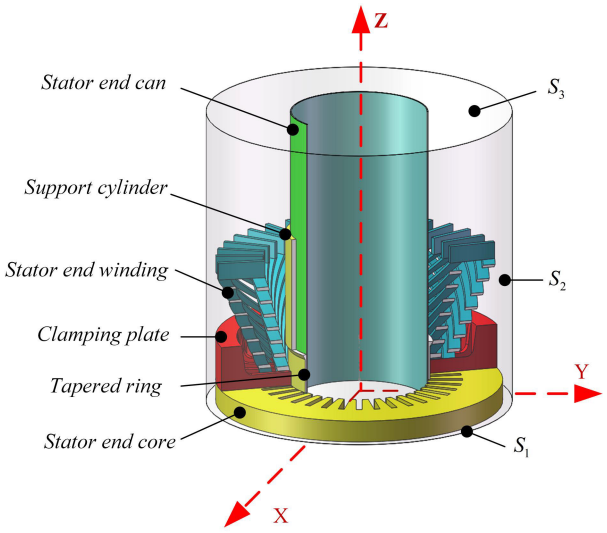

FIGURE 1. 3-D solved region.

TABLE 1. Motor parameters.

Items	Value	Items	Value
Rated power/kW	1500	Rated voltage/kV	6
Rated frequency/Hz	108.5	Number of poles	2
Phase number	3	Winding connection mode	Y
Insulation class	B	Rated speed/rpm	6480
Number of stator winding layers	2	Pitch	14
Number of conductors per slot	8	Number of parallel branches	1

II. HIGH-SPEED CANNED INDUCTION MOTOR END MODEL AND LOSSES CALCULATION METHOD

The solution model of the end structural components of the high-speed canned induction motor is shown in Fig. 1.

The parameters of the motor are shown in Table1.

The stator core is composed of silicon steel sheets with a thickness of 0.5 mm. The stator can is supported on the inner circle of the stator can by the stator core. The stator and rotor can separate from the rotor end region to the stator end region.The stator core is made of silicon steel sheet, which has magnetic anisotropy, but the stator core does not belong to the motor end, so the motor end is not affected by material anisotropy. The principle of contact resistance is that the surface of the structural plane at the two contact points is rough and not smooth, resulting in partial contact on

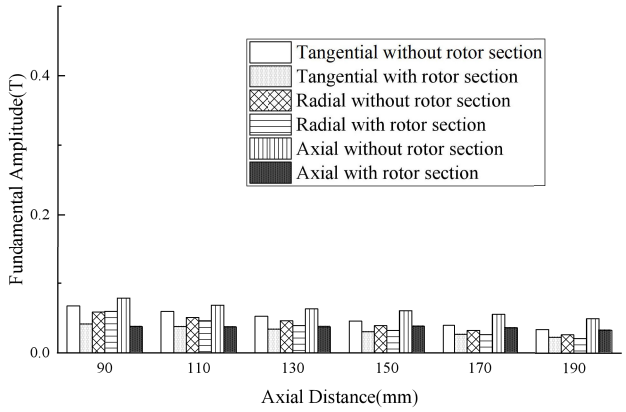

FIGURE 2. Amplitude comparison of air gap fundamental wave with and without rotor section.

TABLE 2. Comparison of calculation time.

Project	Computing time(h)
With rotor section	635.23
Without rotor section	10

the contact surface of the two contact conductive structural parts and no contact on the part, which leads to the contact resistance.To ensure the tightness, the metal structures in contact should be closely combined in this kind of motors, so the influence of contact resistance can be ignored.

The models with and without rotor section are calculated respectively. The fundamental amplitude of the air gap magnetic field of the two models is not much different, as shown in Fig. 2. However, the calculation time of the two models varies greatly, as shown in Table 2. In this paper, the end sealing rings, frames, end rings, and rotor segments are neglected in the established geometric model due to the complex and variable end structure. The effects of the tapered ring and support cylinder, and clamping plate on the circulating current losses and the path of the circulating current losses are mainly studied.

The three-dimensional solution domain Ω at the end of the canned induction motor established in this paper is divided into eddy current area V_1 and non-eddy current area V_2. The eddy-current region includes a stator end can, clamping plate, tapered ring, and support cylinder. The non-eddy current part consists of the stator end core and stator end winding. Taking the vector potential $\dot{\mathbf{A}}$ and the scalar magnetic potential φas unknown functions, the mathematical model of the three-dimensional eddy field at the region of the high-speed canned induction motor is established.

In the eddy-current region V_1:

$$\begin{cases} \mathrm{rot}(\nu\,\mathrm{rot}\dot{\boldsymbol{A}}) - \mathrm{grad}(\nu\,\mathrm{div}\dot{\boldsymbol{A}}) + \mathrm{j}\omega\sigma\dot{\boldsymbol{A}} + \sigma\,\mathrm{grad}\,\dot{\varphi} = 0 \\ \mathrm{div}(-\mathrm{j}\omega\sigma\dot{\boldsymbol{A}} - \sigma\,\mathrm{grad}\,\dot{\varphi}) = 0 \end{cases} \tag{1}$$

In the non-eddy current region V_2:

$$\mathrm{rot}(\nu\,\mathrm{rot}\dot{\boldsymbol{A}}) - \mathrm{grad}(\nu\,\mathrm{div}\dot{\boldsymbol{A}}) = \dot{\boldsymbol{J}} \tag{2}$$

where υ is the magnetic resistivity, ω is the angular frequency, σ is the electrical conductivity, and $\dot{\boldsymbol{J}}_s$ is the source current density.

The boundary conditions satisfied by the three-dimensional eddy current field mathematical model are as follows.

On S_1:

$$\begin{cases} \dot{\boldsymbol{A}} = \dot{\boldsymbol{A}}_0 \\ \dot{\varphi} = \dot{\varphi}_0 \end{cases} \tag{3}$$

OnS2,S3:

$$\begin{cases} \boldsymbol{n}\cdot\dot{\boldsymbol{A}} = 0 \\ (\nu\,\mathrm{rot}\dot{\boldsymbol{A}})\times\boldsymbol{n} = 0 \end{cases} \tag{4}$$

where $\dot{\boldsymbol{A}}_0$ and φ_0 are the initial values of complex vector magnetic potential and complex scalar potential on S1, respectively, $n$is the normal direction of the boundary surface.

During the high-speed rotation of the motor, the magnetic field cuts the structure at the end of the motor to generate the induced electric potential, thus forming the eddy current losses of the structural components themselves. According to classical electromagnetic theory, the eddy current losses density P_e in the solid conductor region is as follow.

$$P_e = \frac{1}{2}\rho\left(\dot{J}\cdot\boldsymbol{J}^*\right) + \frac{1}{2}\rho\,\mathrm{Re}\left(\dot{\boldsymbol{J}}\cdot\dot{\boldsymbol{J}}^{j2\omega t}\right) \tag{5}$$

The average time value of the eddy current losses density P_{eav} in volume V is as follow.

$$\begin{aligned} P_{eav} &= \int_v \frac{1}{2}\rho|\dot{\boldsymbol{J}}|^2\,\mathrm{d}v \\ &= \sum_i^E \int_{vl} \frac{1}{2}\rho_i\left(|j_{xm}|^2 + |j_{ym}|^2 + |\dot{J}_{zm}|^2\right)\mathrm{d}v \\ &= \frac{1}{2}\sum_i^E \rho_i\Big(J_{xmR}^{e\,2} + J_{xmI}^{e\,2} + J_{ymR}^{e\,2} \\ &\quad + J_{ymI}^{e\,2} + J_{zmR}^{e\,2} + J_{zmI}^{e\,2}\Big)\Delta V_i \end{aligned} \tag{6}$$

where $\boldsymbol{J}$ is the eddy current density; ρ is the resistivity; $\Delta V_i$is the volume V of the unit; E represents the total number of units in the volume.

This content can provide the basis for the subsequent calculation of eddy current and circulating current losses.

III. ANALYSIS OF CALCULATION RESULTS

A. EDDY CURRENT LOSS ANALYSIS

The fundamental amplitude of the axial, tangential and radial magnetic fields at each position in the air gap is given along the Z-axis direction. The selection of each position is shown in Fig. 3, and the amplitude is shown in Fig. 4.

It can be seen that the amplitude of the axial magnetic field in the air gap is the largest, followed by the tangential

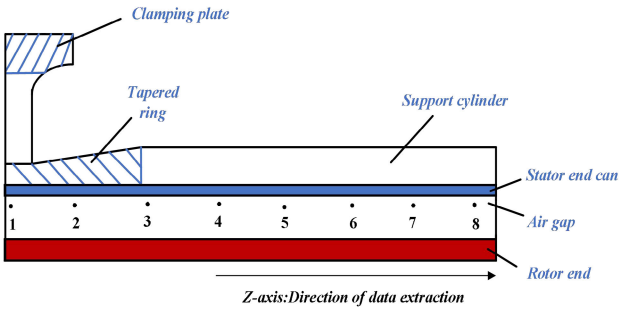

FIGURE 3. Select the position of each point in the air gap.

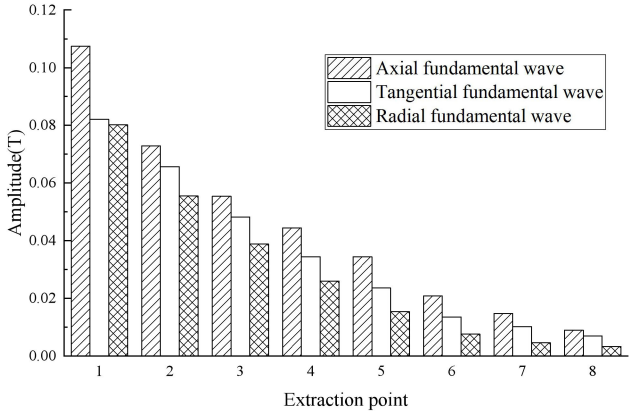

FIGURE 4. Magnetic field distribution at each position of the air gap.

magnetic field, and the amplitude of the radial magnetic field is the smallest.The difference of magnetic field intensity in different directions in different parts of the air gap leads to the difference in the magnetic field distribution at different positions of the structural elements at the end of the motor, which in turn has an impact on the loss path of the structural components. Fig. 5 gives the eddy current paths on the clamping plate, tapered ring, and support cylinder of the end structure.

It can be seen that the distribution of the loss paths on the clamping finger is more influenced by the tangential magnetic field and the clamping ring is more influenced by the axial magnetic field. It can be seen that the eddy currents on the clamping plate flow mainly through the clamping ring and the clamping finger, with the center of the eddy currents, concentrated on the clamping finger. It can be seen from the eddy current paths of the tapered ring and the support cylinder in Fig. 5(c) that the distribution of the loss paths of the tapered ring and the support cylinder is affected by the radial magnetic field, and the eddy current center is slightly farther from the front of the air gap magnetic field. This shows that the magnetic field distribution in the motor end structure is very complex.

B. CIRCULATING CURRENT LOSSES ANALYSIS

The change of the magnetic field at different positions of the air gap with circulating current is shown in the histogram of Fig. 6(a).

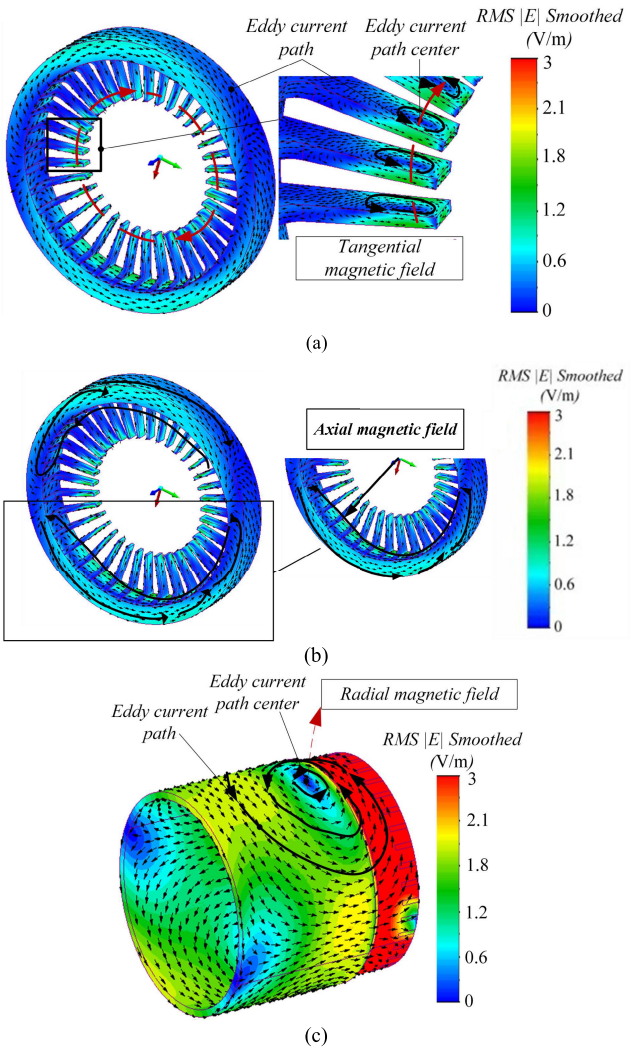

FIGURE 5. Eddy current path of the end structure: (a) Clamping finger eddy current path; (b) Clamping ring eddy current path; (c) Support cylinder and tapered ring eddy current path.

It can be seen that the change trend of the magnetic field in all directions is the same as that when there is only eddy currents. Fig. 6(b) shows the comparison of air gap magnetic field with and without circulating current. From Fig. 6(b), it can be seen that after considering the circulating current, as the air gap position gradually moves away from the stator end winding, the axial magnetic field and radial magnetic field first increase and then decrease, and the tangential magnetic field decreases. Therefore, the circulating current can change the end magnetic field distribution, which in turn affects the loss distribution of the end structure. Fig. 7. gives the circulating current path between the end structural components.

It can be seen that the circulating current path between the tapered ring and support cylinder and the clamping plate is evident in the diagram. The circulating current flows through the clamping finger to the tapered ring and support cylinder and the clamping finger to the clamping plate. This is because

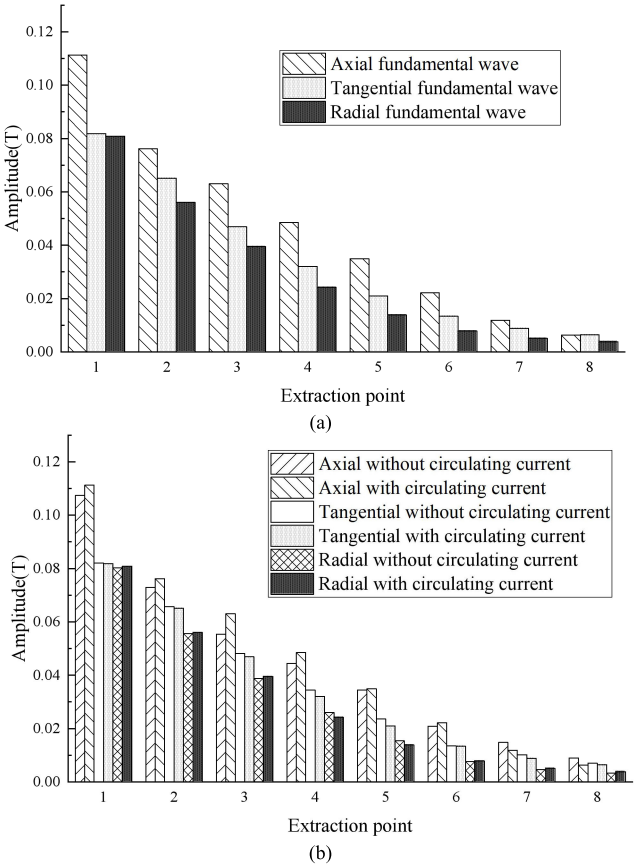

FIGURE 6. Air gap magnetic field distribution in circulating flow conditions: (a) Amplitude of the magnetic field with the circulating current; (b) difference between it only with the eddy current.

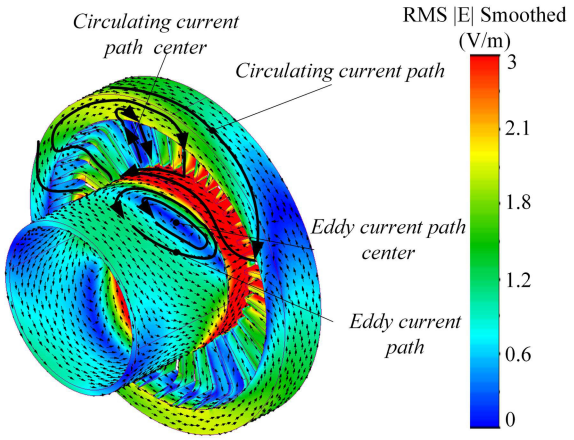

FIGURE 7. Circulating current path between structural components in the end region of the motor.

TABLE 3. End loss-solving conditions for each model.

Project	Support cylinder and tapered ring(S/m)	Clamping plate(S/m)
Model a	1.32×10^6	0
Model b	0	1.37×10^6
Model c	1.32×10^6	1.37×10^6

TABLE 4. End structure losses.

Project	Model a	Model b	Model c
Total loss (W)	3906	322	10065

in the discussion of magnetic fields above, the inclusion of the circulating current has an inhibitory effect on the tangential magnetic field. Therefore there are no obvious eddy current paths on the clamping finger compared to the tapered ring and support cylinder.

The simulation software Magnet is adopted in this paper, which has no insulation boundary conditions. Therefore, the eddy current losses and the circulating current losses in the motor end are calculated by finite element method combined with the superposition method [19]. The corresponding solution conditions are shown in Table 3.

The calculation of model a can obtain the eddy current losses of the tapered ring and the support cylinder itself; the calculation of model b can obtain the eddy current losses of the clamping plate itself; the calculation of model c can obtain not only the circulating current losses between the clamping plate, the tapered ring and the support cylinder,but also the eddy current losses of the clamping plate, the tapered ring and the support cylinder itself. The corresponding calculation results are shown in Table 4.

Through the data analysis in the table, we can see that there are not only the eddy current losses of the structure itself, but also the circulating current losses of the structure at the end of the motor. In this paper, the circulating current losses between the end structures of the motor accounts for 57.99 % of the total loss, which are much larger than the eddy current losses of the end structure.

In this section, it can be verified that the circulating current between the structural components can change the distribution of the magnetic field at the end, which affects the distribution of the circulating current and the eddy current losses. Therefore, it is necessary to analyze the influencing factors of the circulating current of the structural components to suppress the circulating current losses.

C. INFLUENCE OF CLAMPING PLATE RELATIVE PERMEABILITY CHANGE ON CIRCULATING CURRENT PATH

Based on the analysis of previous research, the increase of relative permeability promotes the eddy current losses of end structural components, and the eddy current losses of structural components are not a monotonic function of relative permeability. When the relative permeability of the clamping plate is different, through the calculation of other models, the eddy current losses of the clamping plate,tapered ring, and support cylinder and the circulating current losses between structural components are shown in Table 5.

TABLE 5. End structure losses with different relative permeability.

relative permeability of clamping plate (H/m)	Eddy current losses of clamping plate(W)	Eddy current losses of tapered ring and support cylinder(W)	Circulating current losses (W)
1	322	3906	5837
2	527	3906	6294
5	631	3906	6770
10	750	3906	6749
15	756	3906	6677
20	759	3906	6560

TABLE 6. End structure losses with different conductivity.

Conductivity of clamping plate (S/m)	Eddy current losses of clamping plate(W)	Eddy current losses of tapered ring and support cylinder(W)	Circulating current losses(W)
1.4×10^6	322	3906	5837
1.5×10^6	357	3906	7108
2×10^6	467	3906	7419
3×10^6	552	3906	7649
5×10^6	633	3906	5984
1×10^7	716	3906	5887

The data in Table 5 shows that as the relative permeability of the clamping plate increases, the eddy current losses in the clamping plate itself increases. In contrast, the circulating current losses between the clamping clamping plate, the tapered ring, and the support cylinder first increases and then gradually decreases. This indicates that an inevitable increase in the relative permeability of the end structural components contributes to their own eddy current losses, and that the circulating current losses between the end structural components are more sensitive to changes in relative permeability than the eddy current losses of the structural components themselves.

From the above section, we can see the potential internal distribution of the end structure and the flow direction of the circulating current. The penetration depth represents the attenuation of the electromagnetic field in the structure:

$$d = \sqrt{\frac{1}{\pi \mu \sigma f}} \tag{7}$$

where d is the depth of harmonic penetration; $\mu$is material relative permeability; $\sigma$is material conductivity; $f$is harmonic frequency.

As can be seen from Fig. 8. the depth of harmonic penetration decreases as the relative permeability increases, while at the same time, the path of the circulating current between the clamping plate and the tapered ring changes accordingly. At a relative permeability of 1, the eddy current in the clamping plate flows on its own, while the circulating current flows through the clamping finger to the tapered ring. As the relative permeability increases, not only does the direction of the eddy current flow in the clamping plate itself change, but the circulating current flow to the tapered ring also changes, with most of the circulating current still flowing from the clamping plate to the tapered ring and a small part of the circulating current changing direction and flowing from the tapered ring to the inside of the clamping plate. The high relative permeability material allows the loss path in the end structure to be changed, resulting in reduced end losses in the high-speed canned induction motor. The magnetic field at different positions of the air gap is extracted, and the extraction position is shown in Fig. 9. The difference in tangential and radial magnetic field densities with and without circulating current is shown in Fig. 10.

The magnetic flux flowing through the structure is proportional to the relative permeability. As the relative permeability increases, the leakage flux at the end of the motor is more likely to enter the end structure. Because of the existence of the circulating current, the increase of the magnetic flux in the air gap is suppressed to a certain extent.

D. INFLUENCE OF CLAMPING PLATE CONDUCTIVITY TO CHANGE THE CICULATING CURRENT LOSSES

The change of material conductivity can directly affect the eddy current losses of the structure itself. The eddy current losses on the clamping plate are constantly growing with the increase of the conductivity of the clamping plate. When the conductivity is different, we show the circulating current losses between the corresponding structural components in Table 6.

As seen from the data in the table, as the conductivity of the clamping plate increases, the corresponding resistivity decreases, and the induced current flowing through the structural component increases. There will be more circulating current losses between the end structures. But the circulating current losses between the end structural components do not increase indefinitely. The increase of circulating current will also cause changes in the potential of terminal structures. Therefore, we extracted and analyzed the potential inside the end structural components with different conductivities, and the corresponding data is shown in Fig.11.

From Fig.11, We can see that as the conductivity increases, the potential in the support cylinder and clamping plate changes in the same trend, first decreasing and then slowly increasing. This is because as the conductivity increases, the internal resistance of the clamping plate decreases, and the induced voltage gradually decreases. As the conductivity increases, the potential difference between the structural elements increases. This increases the circulating current between the structural elements and the circulating current losses between the structural components. At the same time, the counter-electromotive force generated by the circulating

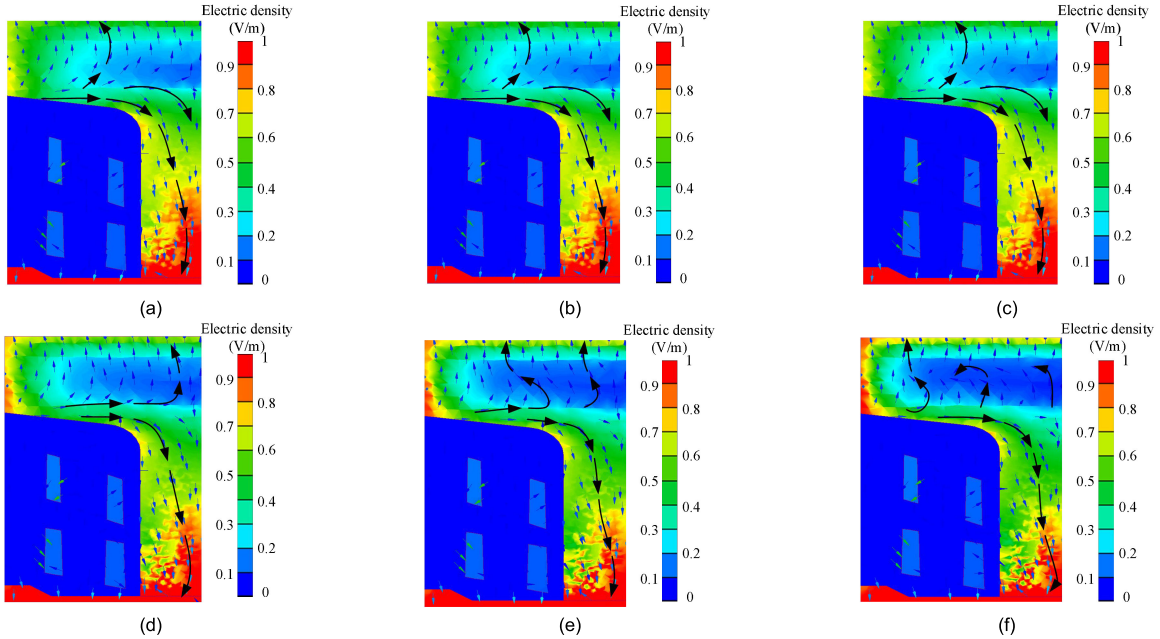

FIGURE 8. Differential circulating current paths of the end structural components when the clamping plate magnetic relative permeability is different: (a) μ =1H/m; (b) μ =2H/m; (c) μ =5H/m; (d) μ =10H/m; (e) μ =15H/m; (f) μ =20H/m.

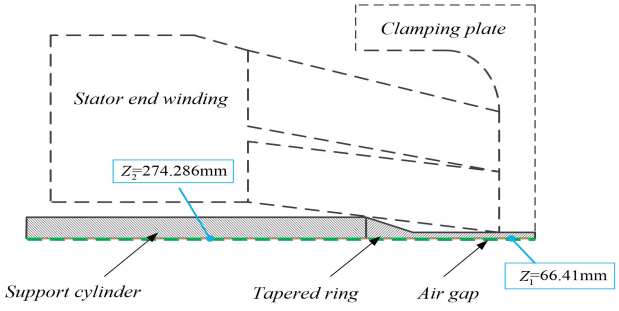

FIGURE 9. Data extraction points.

current increases slowly. The inhibition of circulating current by the magnetic flux gradually becomes apparent. Therefore, the circulating current losses between the clamping plate, the tapered ring, and the support cylinder do not increase indefinitely. The potential distribution at different locations on the structural components is shown in Fig. 12.

It can be seen that the effect of the change in conductivity of the clamping plate on the circulating current path is significantly greater than the effect of the change in relative permeability. The increase in conductivity causes the structural components themselves to change in resistivity. The circulating current is due to the different positions of the clamping plate with the tapered ring and the support cylinder at the end, resulting in different leakage fluxes in the cross-chain. The material properties of the structural components themselves lead to different induced voltages shared by different structural components and a potential difference between the structural components. As the conductivity of the clamping plate increases, the resistance of the clamping plate decreases, resulting in a decrease in the voltage shared by it. The current always flows from the position of high voltage to the position of low voltage, which directly leads to a change in the direction of the circulating current between the structural components.

Fig. 8. and Fig. 12. are mainly used to explain the influence on the circulating current path of the end of the high-speed canned induction motor when the material properties of the end structure change. In the process, the eddy current path of the end structure itself will also change accordingly. After the relative permeability of the clamping plate is increased by 10 times after Fig. 8, the eddy current losses of the clamping plate itself is increased by 1.33 times, while the circulating current losses between structural members is increased by 15.62%. From Fig. 12, it can be seen that with the increasing conductivity of the clamping plate, the eddy current distribution of the clamping plate itself changes, and the circulating current path between the clamping plate and the tapered ring changes.

IV. OPTIMIZED STRUCTURE OF MOTOR END AND ITS BENEFICIAL EFFECT

A. MOTOR END OPTIMIZATION STRUCTURE

From the above study, it can be found that there are eddy not only current losses at the end of the motor but also circulating current losses between the structural components. There are many methods to suppress the eddy current losses, in the end, structural components. Still, the main purpose of this paper is to suppress the circulating current losses between the end structural components. Therefore, effective measures can be taken to block the circulating current path between

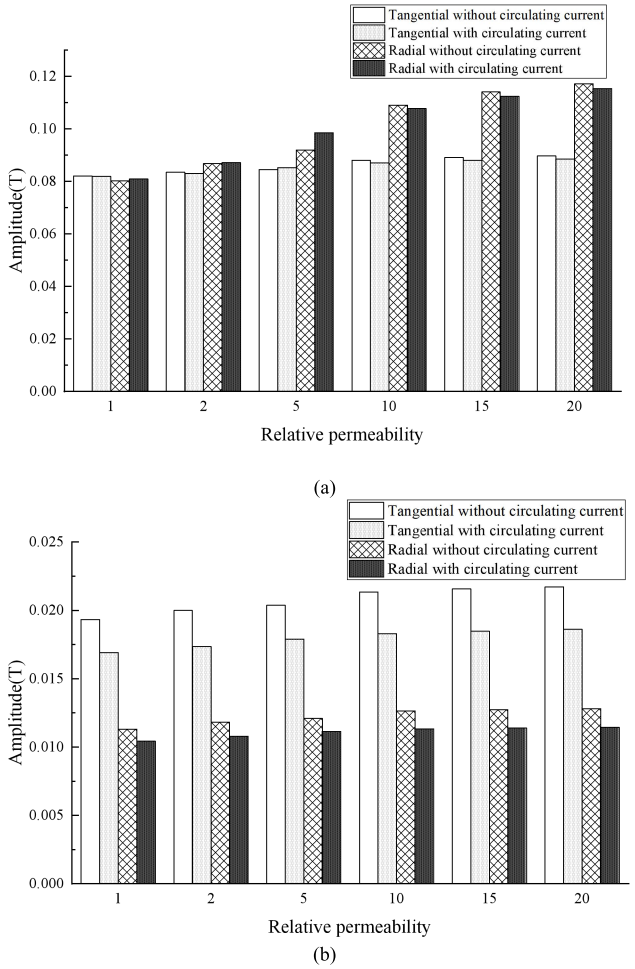

FIGURE 10. Comparison of tangential and radial magnetic density with or without circulating current with different relative permeability of the clamping plate: (a) z = 66 mm; (b) z = 274 mm.

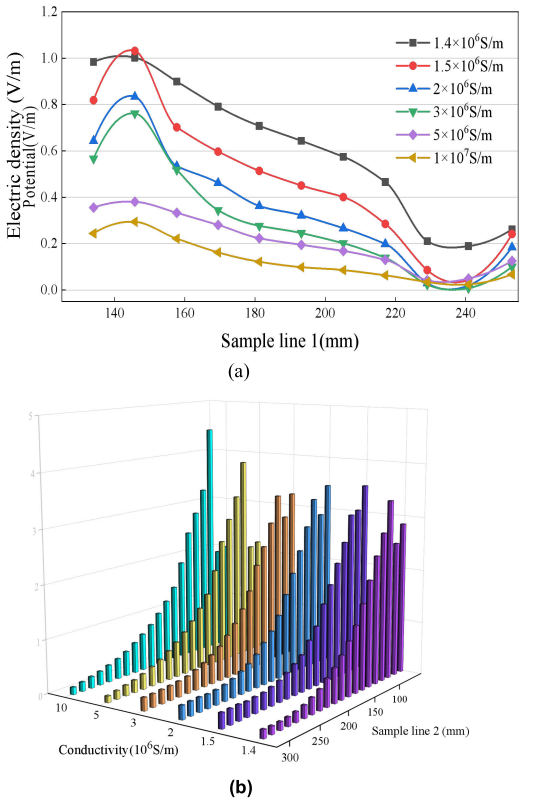

FIGURE 11. Internal potential distribution of the end structure when the conductivity is different: (a) Clamping plate distributions of different conductivity. (b) Tapered ring and support cylinder potential distributions of different conductivity.

TABLE 7. Comparison of end structure component loss.

Projects	Eddy current losses (W)	Circulating current losses(W)
Before clamping plate improvement	322	5837
Two circulation blockers	291	4068
Four circulation blockers	260	2502
Eight circulation blockers	252	1302

the clamping plate, the tapered ring, and the support cylinder, so as to reduce the motor end loss. The selection of the installation position of the circulating current blocker can only play the role of the magnetic force line blocking device effectively when it is installed at the place where the magnetic force lines are concentrated. Therefore, according to the flow path of the magnetic force lines in the end structure of the high-speed canned induction motor during normal operation, the circulating current blocker is placed in the position shown in Fig.13.

It can be seen from Fig.13. that the improved card structure can effectively block the circulating current path of the end structure components. Table 7 gives the compares of the eddy current losses of the end structural components and the circulating current losses between the structural components before and after the clamping plate improvement.

The comparison of the data in Table 7 shows that this scheme has a relatively obvious inhibition effect on the circulating current losses between the end structures, and can completely cut off the original circulating current path between the end structures, directly reducing the circulating current losses of the end structures. After adding four circulating current blockers, the eddy current losses of the clamping plate itself is reduced by 19%, and the circulating current losses between the clamping plate and the tapered ring and the support cylinder is reduced by 47%. This scheme can not only significantly reduce the circulating current losses between structural components, but also reduce the eddy current losses of structural components to a certain extent. When eight circulating current blockers are added, the eddy current losses are reduced very little, and considering the structure and mechanical strength of the clamping plate itself, four circulating current blockers are the most appropriate.

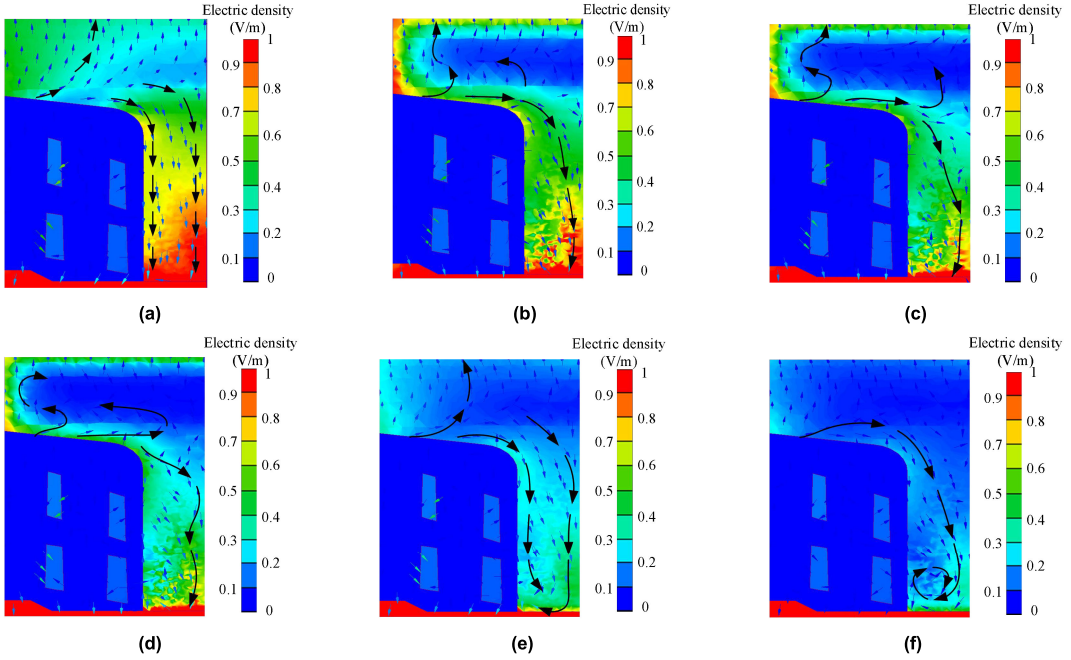

FIGURE 12. Circulating current path of the end structure when the clamping plate conductivity is different: (a) σ =1.4×10^{6}S/m; (b) σ =1.5×10^{6}S/m; (c) σ =2×10^{6}S/m; (d) σ =3×10^{6}S/m; (e) σ =5×10^{6}S/m; (f) σ =1×10^{7}S/m.

B. THE BENEFICIAL EFFECT OF LOSS SUPPRESSION METHOD

The loss is the heat source, and most of the loss will make the internal temperature of the motor rise in the form of heat. Due to the special working environment and mechanical structure of high-speed canned induction motors, the temperature rise effect is more common than that of ordinary motors. To verify that the circulating current is the direct cause of the high magnetic density and abnormal temperature rise at the end of the motor, an end temperature field model is established to analyze the temperature rise.

The steady-state temperature field in the motor is studied numerically, and the basic principle of heat transfer shows that the time term is removed from the heat conduction equation to simplify the difficulty of solving the equation. The three-dimensional steady-state heat-conducting control equation with heat source and anisotropic medium is chosen. In the Cartesian coordinate system, the three-dimensional heat-conducting equation can be expressed as follows:

$$\begin{cases} \dfrac{\partial}{\partial x}(k_x \dfrac{\partial T}{\partial x}) + \dfrac{\partial}{\partial y}(k_y \dfrac{\partial T}{\partial y}) + \dfrac{\partial}{\partial z}(k_z \dfrac{\partial T}{\partial z}) = -q, (x, y, z) \in \Omega \\ \dfrac{\partial T}{\partial n} = 0, (x, y, z) \\ -K \dfrac{\partial T}{\partial n} = \alpha(T - T_f), (x, y, z) \end{cases} \tag{8}$$

where T is the temperature of the end structure to be solved, K, k_x, k_y, k_z is the thermal conductivity of the various materials in the solution domain along the k, y, z direction; q is the sum of the densities of the heat sources in the solution domain; α is the heat dissipation coefficient of the heat dissipation surface; T_f is the temperature of the fluid around

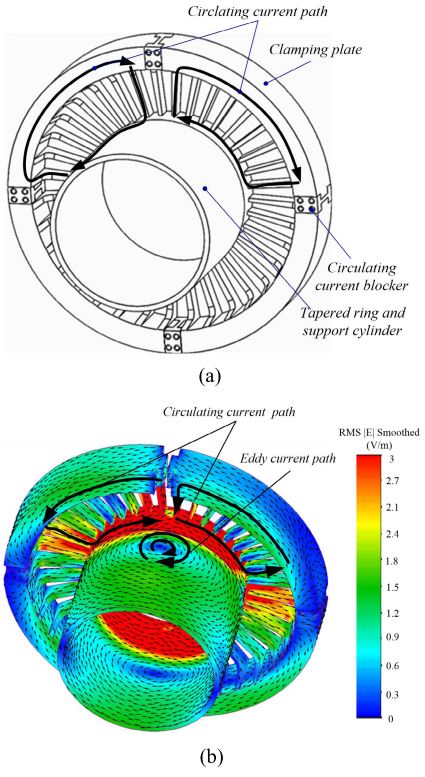

FIGURE 13. Circulating flow path between the end structural components after the clamping plate structure is improved: (a). End-optimized structure; (b). Optimization of loss paths between structural components at the end.

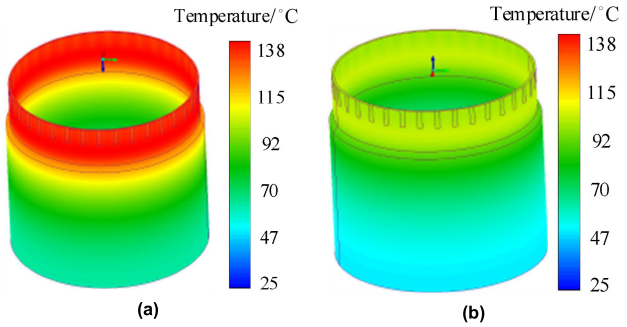

FIGURE 14. Temperature distribution of tapered ring and support cylinder: (a). Temperature distribution before optimization; (b). Temperature distribution after optimization.

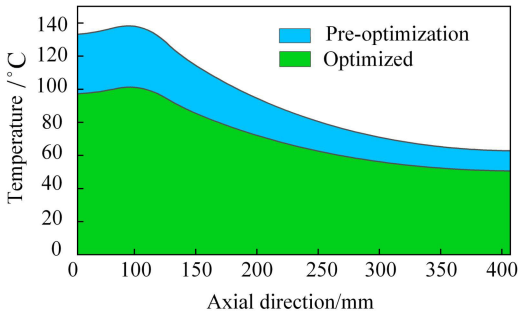

FIGURE 15. Temperature comparison before and after optimization.

the heat dissipation surface. The temperature distribution on the tapered ring and support cylinder after the clamping plate optimization or not is given in Fig.14. and Fig.15. Temperature has little effect on the conductivity of stainless steel materials, so the effect of temperature on the conductivity of materials is ignored [20].

Compared with the structure before optimization, circulating current losses between the structural components after optimization is reduced, and the temperature of each structural component is smaller than that of each structural component before optimization.

V. CONCLUSION

High speed canned induction motor as the research object, the magnetic field of the end region is calculated by the 3-D finite element method. The circulating current losses between end structures are analyzed. The factors of the circulating current path between end structures are discussed.

(1) The loss distribution of the end structural components is mainly influenced by the magnetic field of the air gap. The circulating current flows between the tapered ring, the support cylinder, and the clamping plate, and presents an obvious inhibiting effect on the tangential magnetic field. The circulating current losses between the end structures of the motor accounts for 67.6 % of the total loss, which are much larger than the eddy current losses of the end structure.

(2) The change in material properties of the end structural components can effectively alter the circulating current path between the clamping plate and the tapered ring and support cylinder. The materials with high relative permeability or conductivity can reverse the circulating current between the end structural components, thereby suppressing the circulating current losses between the end structural components and thus reducing the end losses in high-speed canned induction motors.

(3) The circulating current flows between the metal structures at the end of the motor,the addition of the circulating current blocker effectively reduces the end loss of the high-speed canned motor, which shows that the motor loss can be suppressed by blocking the magnetic field or loss path between the structural parts at the end of the motor. Therefore, the circulating current blocker can be added to each metal structure at the end of the motor, such as the tapered ring, support cylinder, stator end can, not only the local overheating problem in the normal operation of the motor can be avoided, but also the safe and reliable operation of the motor can be effectively guaranteed.

REFERENCES

[1] H.-W. Cho, K.-J. Ko, J.-Y. Choi, H.-J. Shin, and S.-M. Jang, "Rotor natural frequency in high-speed permanent-magnet synchronous motor for turbo-compressor application," *IEEE Trans. Magn.*, vol. 47, no. 10, pp. 4258–4261, Oct. 2011.

[2] Y. Liang, L. Gao, C. Li, and Y. Hu, "Investigation of end leakage reactance and its influence on the accuracy in performance calculation of large double canned induction motors," *IEEE Trans. Ind. Electron.*, vol. 65, no. 2, pp. 1420–1428, Feb. 2018.

[3] H. Zhao, H. H. Eldeeb, Y. Zhan, Z. Ren, G. Xu, and O. A. Mohammed, "Robust electromagnetic design of double-canned IM for submergible rim driven thrusters to reduce losses and vibration," *IEEE Trans. Energy Convers.*, vol. 35, no. 4, pp. 2045–2055, Dec. 2020.

[4] L. Gao, Y. Liang, D. Wang, X. Bian, and C. Wang, "Derivation of mathematic model of megawatt double canned induction motors and analysis of its dynamic performance," in *Proc. 22nd Int. Conf. Electr. Mach. Syst. (ICEMS)*, Aug. 2019, pp. 1–4.

[5] H. Chen, F. Yu, W. Yan, and M. Orabi, "Calculation and analysis of eddy-current loss in switched reluctance motor," *IEEE Trans. Appl. Supercond.*, vol. 31, no. 8, pp. 1–4, Nov. 2021.

[6] W. Tong, L. Sun, S. Wu, M. Hou, and R. Tang, "Analytical model and experimental verification of permanent magnet eddy current loss in permanent magnet machines with nonconcentric magnetic poles," *IEEE Trans. Ind. Electron.*, vol. 69, no. 9, pp. 8815–8824, Sep. 2022.

[7] D. Zhang, T. Liu, H. Zhao, and T. Wu, "An analytical iron loss calculation model of inverter-fed induction motors considering supply and slot harmonics," *IEEE Trans. Ind. Electron.*, vol. 66, no. 12, pp. 9194–9204, Dec. 2019.

[8] S. S. Nair, J. Wang, R. Chin, L. Chen, and T. Sun, "Analytical prediction of 3-D magnet eddy current losses in surface mounted PM machines accounting slotting effect," *IEEE Trans. Energy Convers.*, vol. 32, no. 2, pp. 414–423, Jun. 2017.

[9] S. Y. Oh, S.-Y. Cho, J.-H. Han, H. J. Lee, G.-H. Ryu, D. Kang, and J. Lee, "Design of IPMSM rotor shape for magnet eddy-current loss reduction," *IEEE Trans. Magn.*, vol. 50, no. 2, pp. 841–844, Feb. 2014.

[10] J. Cheaytani, A. Benabou, A. Tounzi, M. Dessoude, L. Chevallier, and T. Henneron, "End-region leakage fluxes and losses analysis of cage induction motors using 3-D finite-element method," *IEEE Trans. Magn.*, vol. 51, no. 3, pp. 1–4, Mar. 2015.

[11] N. Taran, D. M. Ionel, V. Rallabandi, G. Heins, and D. Patterson, "An overview of methods and a new three-dimensional FEA and analytical hybrid technique for calculating AC winding losses in PM machines," *IEEE Trans. Ind. Appl.*, vol. 57, no. 1, pp. 352–362, Jan. 2021.

[12] Z. Zhu, Y. Huang, J. Dong, F. Peng, and Y. Yao, "Rotor eddy current loss reduction with permeable retaining sleeve for permanent magnet synchronous machine," *IEEE Trans. Energy Convers.*, vol. 35, no. 2, pp. 1088–1097, Jun. 2020.

[13] Y. Wang, J. Ma, C. Liu, G. Lei, Y. Guo, and J. Zhu, "Reduction of magnet eddy current loss in PMSM by using partial magnet segment method," *IEEE Trans. Magn.*, vol. 55, no. 7, pp. 1–5, Jul. 2019.
[14] J. Ma and Z. Q. Zhu, "Magnet eddy current loss reduction in a 3-slot 2-pole permanent magnet machine," in *Proc. IEEE Int. Electric Mach. Drives Conf. (IEMDC)*, May 2017, pp. 1–8.
[15] K. Yamazaki, "Modeling and analysis of canned motors for hermetic compressors using combination of 2D and 3D finite element method," in *Proc. Int. Electr. Mach. Drives Conf.*, May 1999, pp. 377–379.
[16] L. Gao, J. Wei, C. Li, and Y. Liang, "Analyses on performances of megawatt double-canned induction motors with different can materials," *IEEE Trans. Energy Convers.*, vol. 32, no. 2, pp. 667–674, Jun. 2017.
[17] Q. Yu, X. Wang, and Y. Cheng, "Electromagnetic modeling and analysis of can effect of a canned induction electrical machine," *IEEE Trans. Energy Convers.*, vol. 31, no. 4, pp. 1471–1478, Dec. 2016.
[18] Y. Liang, X. Bian, H. Yu, and C. Li, "Finite-element evaluation and eddy-current loss decrease in stator end metallic parts of a large double-canned induction motor," *IEEE Trans. Ind. Electron.*, vol. 62, no. 11, pp. 6779–6785, Nov. 2015.
[19] S. S. Nair, J. Wang, T. Sun, L. Chen, R. Chin, M. Beniakar, D. Svechkarenko, and I. Manolas, "Experimental validation of 3-D magnet eddy current loss prediction in surface-mounted permanent magnet machines," *IEEE Trans. Ind. Appl.*, vol. 53, no. 5, pp. 4380–4388, Sep. 2017.
[20] S. Sgobba, S. A. E. Langeslag, A. Arauzo, P. Roussel, and P. Libeyre, "Physical properties of a high-strength austenitic stainless steel for the precompression structure of the ITER central solenoid," *IEEE Trans. Appl. Supercond.*, vol. 26, no. 4, pp. 1–4, Jun. 2016.

LIANLIAN GAO was born in 1990. She received the Ph.D. degree in electrical machine from the Harbin University of Science and Technology, Harbin, China, in 2018. She is currently a Lecturer with the Harbin University of Science and Technology.

Her research interests include the research on energy conversion mechanism, analysis and numerical calculation of comprehensive physical field, motor electromagnetic theory, and new technology.

SIMIN WANG was born in Hebei, China, in 1998. She received the bachelor's degree from the Harbin University of Science and Technology, where she is currently pursuing the master's degree in electrical engineering.

Her research interests include electromagnetic field calculation and the circulating current losses of high speed canned induction motor.

JIAJIA LI was born in Henan, China, in 1997. He is currently pursuing the M.S. degree in electrical machines with the Harbin University of Science and Technology, Harbin, China.

His research interests include the analysis of magnetic field and temperature field of high speed canned induction motor.